Chemical Geology 256 (2008) 12–23

Contents lists available at ScienceDirect

Chemical Geology

journal homepage: www.elsevier.com/locate/chemgeo

Geochemistry and Sr–Nd–Pb–Hf isotopes of Early Cretaceous basalts from the Great Xinggan Range, NE China: Implications for their origin and mantle source characteristics

Lian-chang Zhang [a,*], Xin-hua Zhou [b], Ji-feng Ying [b], Fei Wang [b], Feng Guo [c], Bo Wan [a], Zhi-guang Chen [a]

[a] Key Laboratory of Mineral Resources, Institute of Geology and Geophysics, Chinese Academy of Sciences, P.O.BOX 9825, Beijing 100029, China
[b] State Key Laboratory of Lithospheric Evolution, Institute of Geology and Geophysics, Chinese Academy of Sciences, Beijing 100029, China
[c] Guangzhou Institute of Geochemistry, Chinese Academy of Sciences, Guangzhou 510640, China

ARTICLE INFO

Article history:
Received 25 June 2007
Received in revised form 2 July 2008
Accepted 2 July 2008

Editor: R.L. Rudnick

Keywords:
Element geochemistry
Sr–Nd–Pb–Hf isotope
Basaltic rocks
Early Cretaceous
Extensional setting
Great Xinggan Range
NE China

ABSTRACT

Late Mesozoic volcanism is widespread throughout northeastern China, mainly clustering in the Great Xinggan Range, where the major period of volcanic eruption was during the Early Cretaceous. The spatial distribution of volcanic rocks shows a NNE-extending pattern. The lithology of Mesozoic basaltic rocks in the Great Xinggan Range ranges from trachytic basalts, basalts to basaltic andesites. On the basis of lithological associations and spatial relationships, we divide the basalts into four groups, i.e. Tahe, Genhe, Zalute and Xiwu. The Early Cretaceous volcanism in the Great Xinggan Range is characterized by significant large ion lithophile elements (LILE) and light rare earth elements (LREE) enrichment and high field strength elements (HFSE) depletion, with a slightly enriched to depleted Nd–Hf and weakly enriched Sr isotopic compositions (initial $^{87}Sr/^{86}Sr=0.7046–0.7079$, $\varepsilon_{Nd}(t)=+3.6$ to −6.9 and $\varepsilon_{Hf}(t)=+8.9$ to −4.6). The Pb isotopic compositions are also variable with $^{206}Pb/^{204}Pb$, $^{207}Pb/^{204}Pb$ and $^{208}Pb/^{204}Pb$ values of 17.791–18.530, 15.477–15.597 and 37.761–38.497, respectively. The Sr–Nd–Pb–Hf isotopic data indicate that the magmatic sources are heterogeneous, showing an enriched to depleted signature of continental lithospheric mantle. The magmatic sources of the Genhe and Zalute groups are characterized by mixing among PM, EM II and DM, whereas the Tahe and Xiwu groups derive from enriched lithospheric mantle that had experienced metasomatism by fluids or melts from subducted Paleo-Asian and Mongol–Okhotsk ocean slabs and possible influence of Precambrian blocks. The Late Mesozoic volcanic rocks in the Great Xinggan Range resemble those of the Cenozoic calc-alkaline magmatism in the Basin and Range Province of the United States. We therefore suggest that the widespread Mesozoic volcanic rocks in the Great Xinggan Range were generated in an extensional tectonic setting.

1. Introduction

Late Mesozoic volcanic rocks cover a vast area in the Great Xinggan Range and its adjacent areas. Recent studies have shown that ages of these volcanic rocks are mainly Early Cretaceous (Wang et al., 2006; Zhang et al., 2008).

The Late Mesozoic volcanic rocks in the Great Xinggan Range were studied by many authors to investigate the petrology and tectonics setting of the volcanic activity (Zhao et al., 1989; Chen et al., 1997; Lin et al., 1998; Ge et al., 1999; Davis et al., 2001; Yarmolyuk and Kovalenko, 2001; Zhou et al., 2001; Fan et al., 2003; Jahn et al., 2004; Wu et al., 2005). These rocks generally exhibit calc to calc-alkaline affinities and their petrogenesis remains controversial. A mantle plume hypothesis has been proposed to interpret the extensive Late Mesozoic magmatism in the Great Xinggan Range, NE China (Lin et al., 1998; Ge et al., 1999; Shao et al., 1994, 2000; Deng et al., 2004). Fan et al. (2003) and Meng (2003) attributed this magmatic event to a post-orogenic diffuse extension after the closure of the Paleo-Asia and/or Mongol–Okhotsk oceans. Whereas an active continental margin related to the Mesozoic subduction of the Kula or Izanagi Plate has also been put forward (Zhao et al., 1989; Faure and Natal'in, 1992; Zhao et al., 1994; Wu et al., 2005).

In summary, diverse opinions have mainly arisen due to lack of precise and systematic geochemical measurements of these volcanic rocks for the entire Great Xinggan Range. In this paper, we report major, trace element, and Sr–Nd–Pb–Hf isotopic data for the Early Cretaceous basaltic rocks, with aims to understand the geochemical characteristics of the magmatic sources and petrogenesis of these basaltic rocks as well as the regional tectonic setting during the Early Cretaceous.

2. Regional geology and petrography

The Great Xinggan Range is located in the western portion of NE China, south of the Mongol–Okhotsk suture and north of the

* Corresponding author. Tel.: +86 10 82998185; fax: +86 10 62010846.
E-mail address: lczhang@mail.iggcas.ac.cn (L. Zhang).

0009-2541/$ – see front matter © 2008 Elsevier B.V. All rights reserved.
doi:10.1016/j.chemgeo.2008.07.004

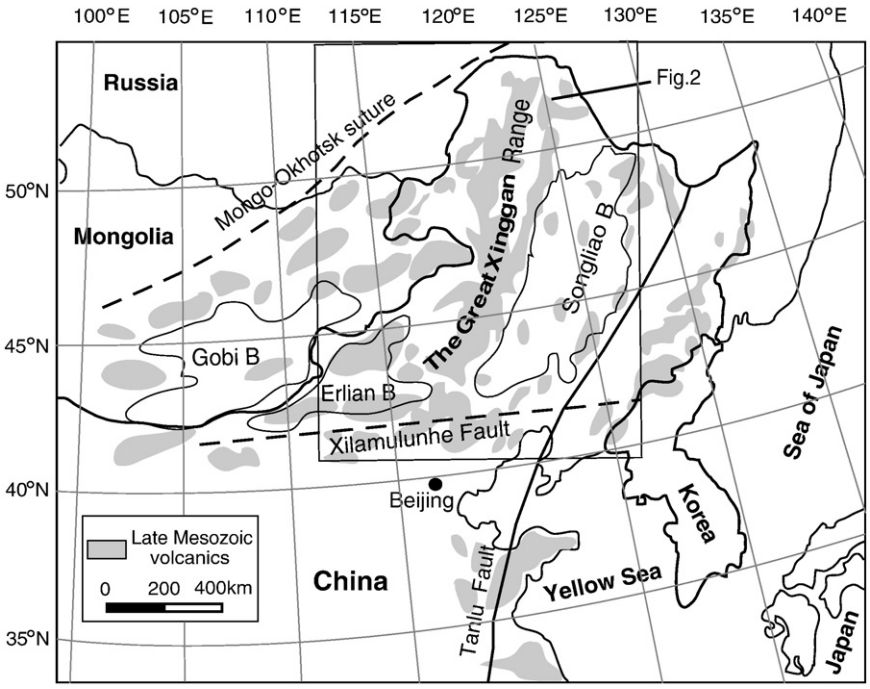

Fig. 1. Geological setting and distribution of volcanic rocks in Northeastern China and its adjacent areas. Modified from Meng (2003).

Xilamulunhe suture (Fig. 1). The Mongol–Okhotsk belt, extending from central Mongolia to the present Gulf of Okhotsk Sea, was formed during the diachronous closure of the Mongol–Okhotsk ocean, which separated the Siberian Craton and the Xinggan Block in the Mid-Jurassic to Early Cretaceous (Van der Voo et al., 1999; Kravchinsky et al., 2002; Tomurtogoo et al., 2005). The Xilamulunhe belt was

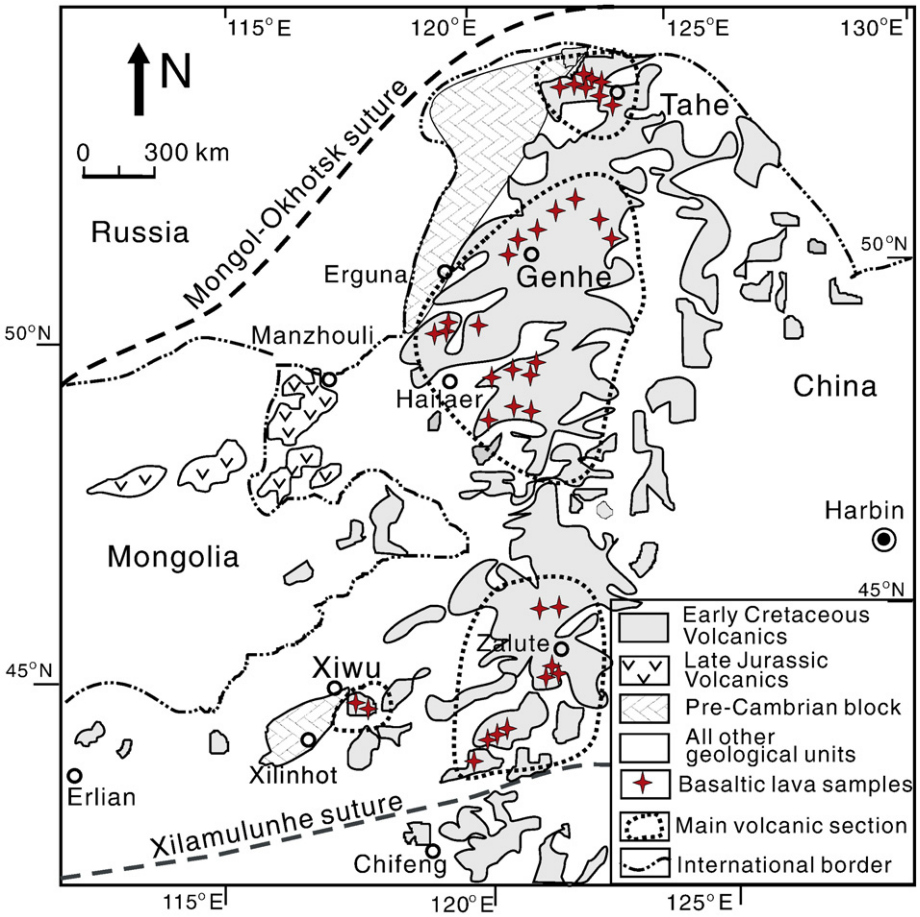

Fig. 2. The sketch of distribution and sampling spots of the Early Cretaceous volcanic rocks in the Great Xinggan Range region.

formed in the course of collision of the Great Xinggan Range and the North China Block during the Late Permian and Early Triassic and marked the final closure of the Paleo-Asian ocean (Mueller et al., 1991; Zorin, 1999; Xiao et al., 2003). The Great Xinggan Range is also accompanied by Late Mesozoic–Cenozoic basin tectonics, including Songliao, Hailar, and Erlan Basins (Meng, 2003).

The Great Xinggan Range region mainly formed from the progressive subduction of the Paleo-Asian ocean and amalgamation of blocks (or terranes) of different types and derivation, and is an important site of juvenile crustal growth during the Phanerozoic (Wu et al., 1999; Chen et al., 2000; Jahn et al., 2001; Badarch et al., 2002; Jahn et al., 2004; Kovalenko, 2004).

There are also several Precambrian blocks present in the region, including Erguna in northern Great Xinggan Range, Xilinhot in southern Great Xinggan Range and Jiamusi in east of Songliao basin between the Siberian and North China Craton (Fan et al., 2003; Xiao et al., 2003; Wu et al., 2002).

The Paleozoic strata, which are mainly composed of low grade metamorphic volcano-sedimentary associations, limestones, and clastic rocks, are sporadically exposed and intruded by voluminous Hercynian, Early-Yanshanian granitic plutons. Along the lithosphere-scale faults are widely distributed ophiolite suites and tectonic nappes of different ages, suggesting that multi-stage oceanic subduction and continent-arc collision occurred during the closure of the Paleo-Asian and Mongol–Okhotsk oceans (Xiao et al., 2003).

Late Mesozoic volcanic rocks cover ~100,000 km^2 with an NE–NNE trend in the Great Xinggan Range, with cumulative thickness of the successions up to ca. 4–5 km (Song and Dou, 1997). The lavas include a wide spectrum of rock types, including basalts, basaltic andesite, trachyte and rhyolite with volcanoclastic units and tuff. Spatially, rhyolite, andesite and their pyroclastic rocks are most widespread. The basaltic sequences are generally divided into two formations based on the lithological associations and lava flow sequence: a) Tamulangou Formation (160–145 Ma), mainly distributed in the western section of the Great Xinggan Range (Chen et al., 2006). b) Yiliekede Formation (125±10 Ma), the majority of volcanism in the Great Xinggan Range erupted in the Early Cretaceous (Fig. 2).

The basaltic rocks of the Yiliekede Formation in the Great Xinggan Range comprise basalt, basaltic andesite, basaltic trachyandesite and trachyandesite. On the basis of lithological associations and spatial relationships, we divide the basalts into four groups (Fig. 2): 1) the Genhe group, distributed in Genhe and Hailar area, is composed mainly of basaltic trachyandesites with a few basaltic andesites, basalts and trachybasalts. The basaltic trachyandesites are porphyritic, with phenocrysts of plagioclase, orthoclase and diopside. The matrix includes fine-grained plagioclase and opaque minerals. 2) the Tahe group, which outcrops to in the west of Tahe town, is composed mainly of basalts and basaltic trachyandesites with a few basaltic andesites. The basalts are commonly subaphyric to weakly porphyritic with predominant phenocrysts of pyroxene and subordinate olivine and plagioclase. The matrix is mainly composed of fine-grained or aphanitic clinopyroxene and plagioclase (<0.2 mm) and opaque oxides. 3) the Zalute group, distributed in the Zalute, Tuquan and Lindong areas, is composed mainly of basaltic andesites, with subordinate basalts and basaltic trachyandesites. The basaltic andesites are porphyritic with phenocrysts of pyroxene, and plagioclase. The matrix includes plagioclase and amphibole and opaque oxides. 4) the Xiwu group, distributed in the Xiwu (near Xilinhot) area, is composed mainly of basaltic trachyandesites.

As shown in Fig. 2 and Table 1, 36 samples of basaltic rocks were collected from the Early Cretaceous lava in the Great Xinggan Range. The samples were mainly distributed in four groups from north to south: Tahe, Genhe, Zalute and Xiwu. The Genhe and Zalute groups constitute the majority of Early Cretaceous volcanism of the north and south Great Xinggan Range, respectively.

3. Analytical methods

All samples were crushed to about mm-scale after removal of weathered rims and handpicked under a magnifier to exclude xenocrysts and amygdules. Only fresh rock chips without xenocrysts and amygdules were selected. These chips were washed in purified water in an ultrasonic bath and crushed in a WC jaw crusher and then powdered in an agate mortar. All of the following analyses were performed at the Institute of Geology and Geophysics, Chinese Academy of Sciences.

Major oxides were analyzed on fused glass disks employing a Phillips PW 1500 X-ray fluorescence spectrometer. The precision and accuracy of the major-element data as determined on the Chinese whole-rock basalt standard GSR-3 (Xie et al., 1989) are ≤3% and ca. 5% (2σ), respectively. The FeO concentration was determined using a conventional titration procedure.

Trace elements were measured by inductively coupled plasma mass spectrometry with a Finnigan MAT Element II mass spectrometer. Samples were dissolved in distilled HF+HNO_3 in 15 ml Savillex Teflon screw-cap beakers and high-pressure Teflon bombs at 120 °C for 6 days, dried and then diluted to 50 ml for analysis. A blank solution was prepared and the total procedural blank was <50 ng for

Table 1
Samples of the Early Cretaceous basaltic rocks in the Great Xinggan Range

No.	Sample no.	Locations	Name	Age (Ma)
Genhe group				
1	ZLT04-9	48°00′18″N/122°48′23″E	Basaltic andesite	122.2±0.6[a]
2	ZLT04-10	48°01′25″N/123°00′23″E	B-T andesite	
3	YKS04-3	48°50′47″N/121°34′58″E	B-T andesite	106.2±0.6[a]
4	YK04-1	49°12′22″N/120°56′59″E	B-T andesite	114.3±1.0[a]
5	YK04-3	49°12′22″N/120°56′59″E	B-T andesite	
6	YK04-4	49°12′22″N/120°36′59″E	B-T andesite	115.8±0.6[a]
7	EBY04-1	49°50′32″N/119°57′34″E	B-T andesite	139.7±0.7[a]
8	EBY04-2	49°50′32″N/119°57′34″E	B-T andesite	
9	EBY04-4	49°50′47″ N/119°57′37″E	B-T andesite	140.3±0.7[a]
10	ER04-7	49°50′32″N/119°57′34″E	B-T andesite	
11	ESH04-2	50°24′02″N/120°12′02″E	B-T andesite	
12	GH04-1	50°21′32″N/120°26′49″E	Trachybasalt	123.9±0.6[a]
13	GH04-3	50°44′55″N/121°02′22″E	B-T andesite	
14	GH04-4	50°59′17″N/121°19′16″E	B-T andesite	114.5±0.6[a]
15	JGD04-3	50°22′30″N/124°13′28″E	Basaltic andesite	
16	JGD04-4	49°56′53″N/124°22′48″E	Basalt	115.3±0.6[a]
Tahe group				
17	05TH05	52°19′30″N/124°40′39″E	B-T andesite	
18	05TH10	52°22′44″N/124°41′16″E	Basalt	123.7±0.6[a]
19	05TH11	52°27′42″N/124°38′31″E	Basalt	
20	05TH19	52°34′18″N/124°33′33″E	B-T andesite	
21	05TH21	52°34′18″N/124°33′33″E	B-T andesite	122.3±0.6[a]
22	05TH23	52°39′38″N/124°19′38″E	Basaltic andesite	
23	05TH25	52°39′38″N/124°20′38″E	B-T andesite	125.6±0.6[a]
24	05TH26	52°39′38″N/124°21′39″E	B-T andesite	
25	05TH27	52°39′38″N/124°22′40″E	B-T andesite	
Zalute group				
26	ZHJ04-1	44°45′12″N/121°07′51″E	Basaltic andesite	122.8±0.6[b]
27	ZHJ04-4	44°45′118″N/121°07′51″E	Basaltic andesite	
28	XFZH-04	43°52′34″N/118°53′39″E	Basalt	121.0±2.0[b]
29	MAN-1	44°26′56″N/120°48′04″E	Basaltic andesite	
30	MAN-2	44°26′56″N/120°48′01″E	Basaltic andesite	
31	MAN-3	44°27′02″N/120°47′49″E	Basaltic andesite	
32	LD-05	43°55′45″N/119°26′46″E	Basaltic andesite	131.2±0.7[b]
33	LD-06	43°55′45″N/119°26′46″E	Basaltic andesite	
34	LD-10	43°55′46″N/119°26′09″E	Basaltic andesite	
Xiwu group				
35	XW04-1	44°18′54″N/117°39′08″E	B-T andesite	121.5±0.6[b]
36	XW04-4	44°18′54″N/117°38′42″E	B-T andesite	

B-T andesite, basaltic trachyandesite.
[a]Ar–Ar ages from Wang et al., 2006.
[b]Ar–Ar ages from Zhang et al., 2008.

all trace elements. Indium was used as an internal standard to correct for matrix effects and instrument drift. Precision for all trace elements is estimated to be 5% and accuracy is better than 5% for most elements by analyses of the GSR-3 standard (Xie et al., 1989; Zhang et al., 2008). The results of major and trace elements are listed in Table 2 and Supplementary Table S1.

Sr–Nd–Pb isotopic data were measured on a MAT 262 mass spectrometer. The Sr and Nd isotope ratios were respectively normalized to $^{86}Sr/^{88}Sr=0.1194$ and $^{146}Nd/^{144}Nd=0.7219$. The La Jolla standard yielded $^{143}Nd/^{144}Nd=0.511862\pm10$ (2 sigma, $n=13$) and NBS-987 gave $^{87}Sr/^{86}Sr=0.710240\pm11$ (2 sigma, $n=6$). The $^{87}Rb/^{86}Sr$ and $^{147}Sm/^{144}Nd$ ratios were calculated using the Rb, Sr, Sm and Nd abundances. The initial $^{87}Sr/^{86}Sr$ and $^{143}Nd/^{144}Nd$ ratios were calculated using their whole-rock mean Ar–Ar ages of 125 Ma for Yiliekede Formation. Pb isotopic ratios were also obtained on the Finnigan MAT-262. Measured Pb isotopic ratios were corrected for instrumental mass fractionation of 0.1% per atomic mass unit by references to repeated analyses of the NBS-981 Pb standard. Repeated analyses of NBS-981 gave $^{204}Pb/^{206}Pb=0.05897\pm15$, $^{207}Pb/^{206}Pb=0.91445\pm80$, $^{208}Pb/^{206}Pb=2.16170\pm180$ (2 sigma). Total blank levels were below 0.2 ng for Rb, Sr, and Nd, and around 0.5 ng for Pb. The results are listed in Supplementary Table S2.

For the Hf isotope analysis, about 100 mg rock powder and 200 mg $Li_2B_4O_7$ were mixed homogeneously, the mixture was digested in a Pt–Au alloy crucible at 1200 °C for fifteen minutes in a high-frequency furnace. The quenched alkali bead was dissolved in 2 mol/L HCl. Hf fraction was separated by using a modified single-column Ln extraction chromatography method (Li et al., 2005). Hf isotopes were determined using a Finnigan Neptune Multicollector inductively coupled plasma mass spectrometer. The measured $^{176}Hf/^{177}Hf$ ratios were normalized to $^{179}Hf/^{177}Hf=0.7325$, and the reported $^{176}Hf/^{177}Hf$ ratios were further adjusted relative to the JMC 475 standard of 0.282160. During the course of this study, basalt standards BHVO-2 and JB-1 yield $^{176}Hf/^{177}Hf$ ratios of 0.283098 ± 5 (2 sigma, $n=5$) and 0.282959 ± 16 (2 sigma, $n=5$), respectively. These values agree well within analytical errors with the previous results (Kleinhanns et al., 2002; Bizzarro et al., 2003). The results are listed in Supplementary Table S2.

4. Results

4.1. Major elements

The Early Cretaceous basaltic rocks in the Great Xinggan Range plot as basalt, trachybasalt, basaltic trachyandesites and basaltic andesite on a SiO_2 vs. K_2O+Na_2O classification diagram of Le Bas et al. (1986) (Fig. 3A). The diagram shows that the basalts span a range of 47.3–51.8 wt.% SiO_2 with MgO of 4.15–8.11 wt.%, the trachybasalt has SiO_2 of 49.8 wt.% with Na_2O of 3.54 wt.% and K_2O of 2.23 wt.%, the basaltic trachyandesites have 51.9–55.8 wt.% SiO_2 with 3.08–6.13 wt.% Na_2O

Table 2
Major oxide compositions (wt.%) of the Early Cretaceous basaltic rocks in the Great Xinggan Range

Sample no.	SiO_2	TiO_2	Al_2O_3	Fe_2O_3	FeO	MnO	MgO	CaO	Na_2O	K_2O	P_2O_5	LOI	Total	Mg#
Genhe group														
ZLT04-9	53.97	0.99	16.49	6.19	3.99	0.12	4.23	7.16	3.12	1.53	0.30	2.15	100.24	0.45
ZLT04-10	52.03	1.05	16.74	6.30	4.80	0.14	5.28	5.40	4.36	1.78	0.32	2.03	100.23	0.46
YKS04-3	53.38	1.98	15.32	5.45	3.65	0.13	4.14	7.13	3.58	1.86	1.06	2.38	100.06	0.47
YK04-1	52.81	1.92	15.22	4.21	5.59	0.18	4.05	6.29	3.22	2.87	1.07	2.25	100.06	0.36
YK04-3	53.03	1.93	15.41	3.61	6.25	0.16	4.18	6.31	3.24	2.80	1.05	2.13	99.69	0.34
YK04-4	53.39	1.95	15.35	4.65	5.59	0.19	3.86	6.26	3.44	2.77	1.07	1.73	100.10	0.35
EBY04-1	52.63	1.33	16.04	6.47	3.18	0.11	4.40	6.37	3.84	3.02	0.63	1.98	100.00	0.52
EBY04-2	55.60	1.32	16.19	4.77	2.75	0.12	4.21	4.68	3.84	3.08	0.64	2.70	99.90	0.54
EBY04-4	55.83	1.27	15.90	5.00	2.70	0.09	3.02	4.74	3.62	3.79	0.58	3.53	100.06	0.46
ER04-7	52.87	1.13	16.87	6.36	2.70	0.12	4.59	5.83	3.64	2.92	0.47	2.48	99.99	0.57
ESH04-2	55.56	1.17	18.38	4.65	3.06	0.07	2.71	3.27	6.13	2.14	0.41	2.57	100.12	0.41
GH04-1	49.76	1.68	17.37	5.05	3.82	0.16	5.27	7.94	3.54	2.23	0.56	2.28	99.66	0.52
GH04-3	54.47	1.16	16.13	6.97	2.57	0.16	4.49	4.37	3.75	3.19	0.38	2.15	99.78	0.57
GH04-4	53.85	1.30	17.57	4.30	3.58	0.17	4.54	3.90	5.01	3.46	0.38	2.28	100.34	0.49
JGD04-3	54.01	1.05	16.87	4.83	3.95	0.14	4.87	6.41	3.30	1.23	0.34	2.75	99.74	0.49
JGD04-4	48.55	1.21	15.99	4.04	5.21	0.15	7.55	8.97	2.84	1.93	0.52	2.45	99.41	0.53
Tahe group														
05TH05	53.63	1.08	18.6	5.30	2.93	0.14	3.57	5.48	3.30	3.14	0.32	2.40	99.89	0.48
05TH10	47.34	1.51	17.89	4.69	5.99	0.17	6.01	9.50	3.03	1.25	0.44	1.55	99.37	0.44
05TH11	47.78	1.33	17.44	3.70	6.38	0.16	6.92	9.11	3.17	1.46	0.37	1.65	99.47	0.46
05TH19	52.87	1.09	16.27	5.33	2.53	0.09	4.96	7.13	4.22	1.87	0.31	3.25	99.92	0.60
05TH21	52.93	1.1	16.16	5.14	2.71	0.11	5.15	7.19	4.35	1.88	0.29	3.21	100.22	0.59
05TH23	54.59	1.04	17.76	4.93	4.23	0.14	4.40	7.08	2.74	1.72	0.34	0.43	99.40	0.45
05TH25	52.65	1.48	16.19	5.74	3.75	0.12	3.23	7.62	3.08	2.05	0.59	2.81	99.31	0.40
05TH26	52.62	1.52	16.28	5.28	3.19	0.12	3.37	7.99	3.2	2.08	0.61	3.73	99.99	0.45
05TH27	53.47	1.56	16.27	5.87	2.52	0.10	3.60	6.83	3.95	2.15	0.64	2.48	99.44	0.52
Zalute group														
ZHJ04-1	56.80	1.06	16.87	6.17	2.61	0.18	3.48	5.35	3.81	2.35	0.23	1.38	100.28	0.52
ZHJ04-4	56.33	0.96	16.79	6.23	2.43	0.11	3.69	5.28	3.78	2.43	0.22	1.55	99.80	0.53
XFZH-04	51.02	1.46	16.89	5.67	2.76	0.15	6.89	8.39	3.67	1.07	0.48	1.33	99.77	0.66
MAN-1	56.84	1.01	16.57	2.43	5.97	0.13	3.9	6.35	3.59	1.49	0.26	1.48	100.02	0.34
MAN-2	56.71	0.96	16.82	3.03	4.62	0.13	3.81	6.34	3.44	2.01	0.25	1.12	99.23	0.39
MAN-3	56.76	1.02	16.39	2.17	5.51	0.13	4.03	6.38	3.37	1.87	0.26	1.27	99.15	0.36
LD-05	53.68	0.93	18.78	6.78	2.89	0.19	3.04	9.47	3.03	0.49	0.27	0.30	99.45	0.46
LD-06	53.46	0.93	17.77	6.84	3.35	0.19	3.72	9.87	3.16	0.36	0.26	0.28	99.99	0.48
LD-10	53.14	0.89	18.04	6.34	3.46	0.18	3.5	9.2	3.38	0.45	0.24	0.02	98.85	0.42
Xiwu group														
XW04-1	54.57	1.94	15.50	3.74	5.28	0.15	3.40	6.14	3.43	2.47	0.74	2.12	99.48	0.33
XW04-4	52.58	2.23	15.40	4.67	5.95	0.17	3.73	6.52	3.54	2.24	1.01	2.22	100.26	0.33

All samples were analyzed by the X-ray fluorescence method at the Institute of Geology and Geophysics, Chinese Academy of Sciences.

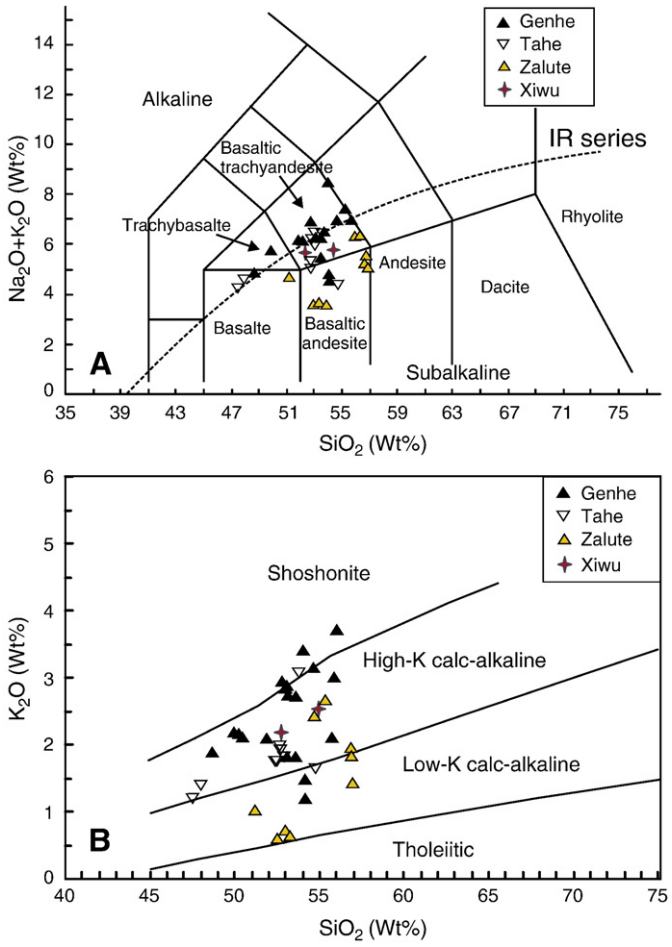

Fig. 3. (A) SiO_2 vs. K_2O+Na_2O classification diagram and (B) K_2O vs. SiO_2 plots of the Late Mesozoic volcanic rocks in the Great Xinggan Range (Le Bas et al., 1986). The boundary (IR series) between alkaline and subalkaline series is from Irvine and Baragar (1971).

and 1.78–3.79 wt.% K_2O, and the basaltic andesites have 54.0–56.8 wt.% SiO_2 and 4.23–4.87 wt.% MgO.

On the SiO_2 vs. K_2O+Na_2O diagram (Fig. 3A), the Genge and Tahe basaltic rocks are relatively dispersed, plotting in the fields of trachybasalt, basaltic trachyandesite, basalt and basaltic andesite. The Zalute and Xiwu basaltic rocks are similar to sub-alkaline series including basalt, basaltic andesite and basaltic trachyandesite. In a SiO_2 vs. K_2O diagram (Fig. 3B), the Genhe and Tahe basaltic rocks are relatively dispersed and plot in the high-K calc-alkaline and shoshonite series fields while the Zalute and Xiwu basaltic rocks fall in high-K calc-alkaline and low-K calc-alkaline series.

The four groups display obvious differences in oxide compositions (Table 3). The Zalute basaltic rocks have lower K_2O, alkaline (K_2O+Na_2O) contents and K_2O/Na_2O ratio than those of the Genhe group. The Genhe group basalts have higher K_2O, alkaline contents and K_2O/Na_2O ratios. The Tahe and Xiwu basaltic rocks lie between the Genhe and Zalute group basalts in terms of major elements. However, the Genhe basalts show higher Al_2O_3 contents and the Xiwu samples show higher TiO_2 contents.

In Harker diagrams (Fig. 4), K_2O contents of the basaltic rocks display positive correlations with SiO_2 contents, whereas MgO, TFeO ($FeO+Fe_2O_3$) and CaO contents exhibit negative correlations, Na_2O and TiO_2 contents show no correlation with SiO_2 contents.

4.2. Trace elements

Based on chondrite-normalized REE patterns and primitive mantle normalized spidergrams, the basaltic rocks are also divided into four groups (Fig. 5).

Although REE patterns of the four groups share some common features, such as enrichment of LREE relative to HREE (Fig. 5A–D) and lack of obvious Eu anomalies, they exhibit also some differences (Table 3). The Zalute rocks have lower ΣREE and $(La/Yb)_N$, with ΣREE ranging between 60–127 ppm (average = 100 ppm) and $(La/Yb)_N$ = 2.80–7.00 (average = 5.20), compared to ΣREE 93–324 ppm (217 ppm) and $(La/Yb)_N$ 6.81–39.52 (16.9) of the Genhe rocks. The Tahe rocks are between those of the Genhe and Zalute for ΣREE and $(La/Yb)_N$. Whereas the Xiwu rocks show the highest ΣREE and $(La/Yb)_N$, with 233–298 ppm (265 ppm) and 19.95–27.75 (20.35), respectively.

In the primitive mantle normalized spidergrams (Fig. 5E–H), all of the samples display LILEs, LREE enrichment and significant Nb–Ta depletion, distinct from MORB, OIB and CFB that show no or insignificant HFSE anomalies (Smedley, 1986; Sun and McDonough, 1989). Samples from the Genhe and Xiwu have lower Ba/La and Th/La ratios than those of Zalute, while those values for the Tahe samples fall between the Genhe and Zalute rocks. The Genhe, Xiwu and Zalute rocks have similar Nb/La ratios. The Tahe rocks have the lowest Nb/La ratios among the four groups while these values for the other three groups are similar (Fig. 6).

4.3. Sr–Nd–Pb–Hf isotopes

Except for the samples from Xiwu and Tahe, most of the Early Cretaceous basaltic rocks from the Genhe and Zalute display similar Sr and some different Nd isotopic ratios (Supplementary Table S2). The majority of samples of the Genhe spans an initial $^{87}Sr/^{86}Sr$ range of 0.7046–0.7059 and a $\varepsilon_{Nd}(t)$ range of 1.0–3.6. Samples from the Zalute spans an initial $^{87}Sr/^{86}Sr$ range of 0.7047–0.7079 and a $\varepsilon_{Nd}(t)$ range of −1.0 to +2.6. In contrast, the Tahe and Xiwu rocks have much higher initial Sr isotopic compositions with $(^{87}Sr/^{86}Sr)_i$ = 0.7055–0.7079 and 0.7055–0.7061, respectively, and lower Nd isotopic compositions with $\varepsilon_{Nd}(t)$ = +0.3 to −6.9 and −1.2 to −6.5, respectively. These samples have similar Nd model ages (T_{DM} = 0.6–1.3 Ga, Supplementary Table S2).

In the $(^{87}Sr/^{86}Sr)_i$ vs. $\varepsilon_{Nd}(t)$ variation diagram (Fig. 7A), some Genhe and Zalute samples plot near primitive mantle (PM) composition, the

Table 3
Geochemical differences among Genhe, Tahe, Zalute and Xiwu basaltic rocks on some major elements and REE

	Genhe (n=16)		Tahe (n=9)		Zalute (n=9)		Xiwu (n=2)	
	Range	Average	Range	Average	Range	Average	Range	Average
Al_2O_3 (wt.%)	15.22–18.38	16.37	16.16–18.60	16.98	16.39–18.04	17.21	15.40–15.50	15.45
K_2O (wt.%)	1.23–3.79	2.54	1.25–3.14	1.96	0.36–2.43	1.39	2.24–2.47	2.36
K_2O+Na_2O	4.53–8.47	6.32	4.28–6.44	5.40	3.52–6.21	4.86	5.78–5.90	5.84
K_2O/Na_2O	0.37–1.05	0.69	0.41–0.75	0.58	0.11–0.64	0.39	0.63–0.72	0.68
MgO (wt.%)	2.71–7.55	4.46	3.23–6.92	4.58	3.04–6.89	4.01	3.40–3.73	3.57
TiO_2 (wt.%)	0.99–1.98	1.40	1.08–1.56	1.30	0.89–1.46	1.02	1.94–2.23	2.09
ΣREE (ppm)	93–324	217	101–208	155	60–127	100	233–298	265
(La/Yb)N	6.81–39.52	16.9	9.24–21.16	14.6	2.80–7.00	5.2	17.95–22.75	20.35

n, sample data; $(La/Yb)_N$, Chondrite-normalizing values from Boynton (1984).

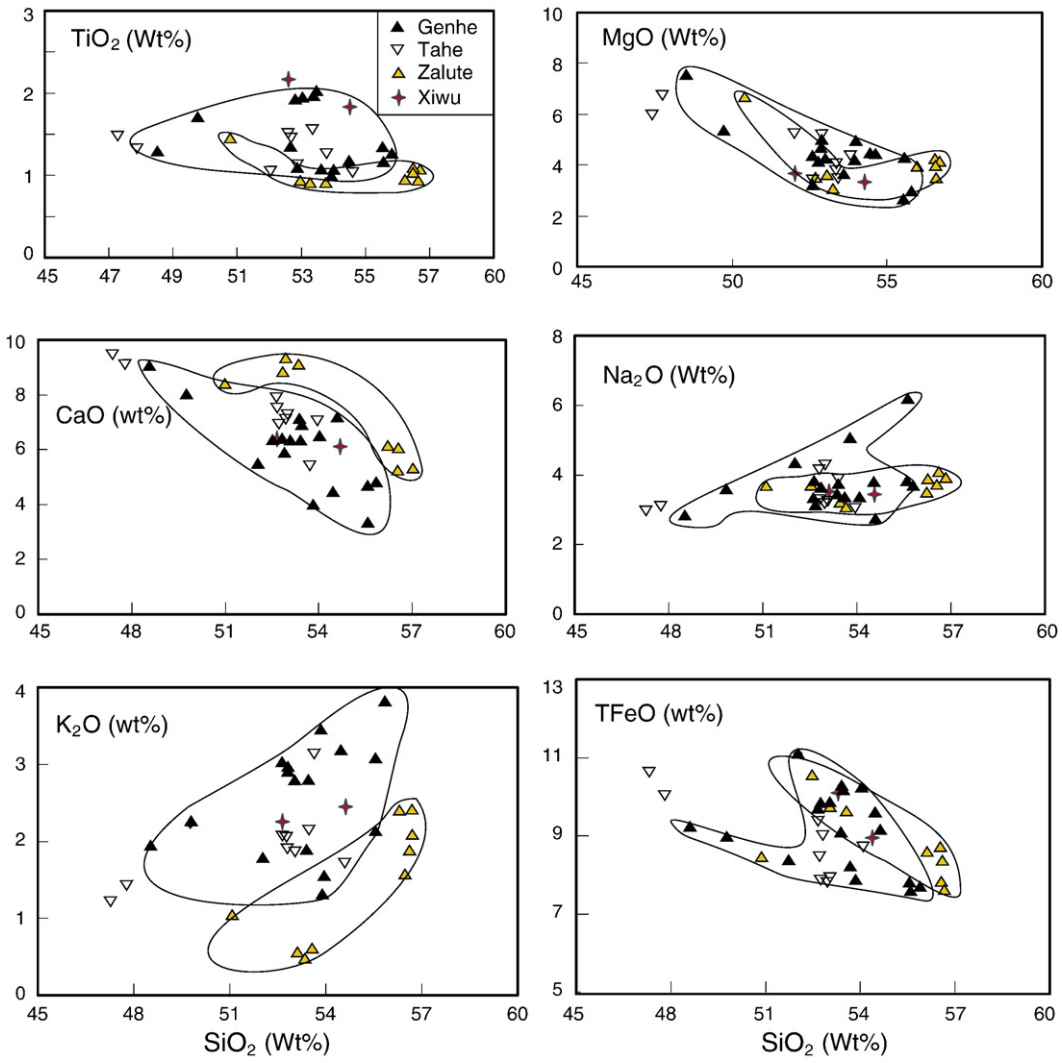

Fig. 4. Harker diagrams of the Late Mesozoic volcanic rocks in the Great Xinggan Range. All major oxides are loss-free normalized to 100%. Symbol as in Fig. 3.

Tahe and Xiwu samples plot among PM, EM I and EM II, but all samples plot in a field defined by IAB, and are close to the Cenozoic basalts from the Basin and Range Province of the United States (Hawkesworth et al., 1995; Rogers et al., 1995).

The Genhe and Zalute samples have positive $\varepsilon_{Hf}(t)$ values clustering around +4.1 to +8.9, whereas the Xiwu and Tahe have low positive to negative $\varepsilon_{Hf}(t)$ values between +1.9 and −4.6. There is a clear positive correlation between $\varepsilon_{Hf}(t)$ and $\varepsilon_{Nd}(t)$ values. All Nd–Hf isotopic values plot near the terrestrial array line and within the range of OIB (Fig. 7B). The higher $\varepsilon_{Hf}(t)$ values of the Genhe and Zalute groups may represent the Hf isotopic composition of its mantle source. However, these values are lower than those of synchronous MORB-type depleted mantle ($\varepsilon_{Nd}(t)\approx+8$ and $\varepsilon_{Hf}(t)\approx+13$), but similar to those of OIB+IAV type mantle (Fig. 7B).

The $^{206}Pb/^{204}Pb$, $^{207}Pb/^{204}Pb$ and $^{208}Pb/^{204}Pb$ values of the Early Cretaceous basaltic are 17.791–18.530, 15.477–15.597 and 37.761–38.497, respectively (Supplementary Table S2). In $^{208}Pb/^{204}Pb$ vs. $^{206}Pb/^{204}Pb$ and $^{207}Pb/^{204}Pb$ vs. $^{206}Pb/^{204}Pb$ isotope correlation diagrams, all samples plot above the northern hemisphere reference line (NHRL). The Genhe, Zalute and Xiwu rocks exhibit remarkable distinctions in $^{206}Pb/^{204}Pb$, $^{207}Pb/^{204}Pb$ and $^{208}Pb/^{204}Pb$ values. The Genhe rocks have lower $^{208}Pb/^{204}Pb$ and $^{207}Pb/^{204}Pb$ values than Zalute, whereas the Xiwu rocks have the lowest $^{206}Pb/^{204}Pb$ values (Fig. 8A and B). In Pb–Nd and Pb–Hf isotopic diagrams all samples plot betwween MORB, EMI and EMII (Fig. 9A and B).

5. Discussion

5.1. Attribute of basaltic rocks

The Late Mesozoic basaltic rocks in the Great Xinggan Range are mainly composed of trachytic basalts–basalts–basaltic andesites and these rocks were classified into four groups in terms of their lithology and spatial relationships, namely the Genhe and Tahe groups in the northern Great Xinggan Range and the Zalute and Xiwu groups in the southern Great Xinggan Range. The basaltic rocks from the north Great Xinggan Range trends to be alkaline, whereas those of the south Great Xinggan Range are subalkaline (Fig. 3).

The Genhe and Tahe rocks in the northern Great Xinggan Range are highly enriched in LILEs and LREE, with contents similar to those of intraplate alkaline basalts. However, they resemble volcanic arc calc-alkline basalts in the obvious depletion of the HFSE (Fig. 5A, B and E, F). The Zalute and Xiwu rocks in the southern Great Xinggan Range are similar to volcanic arc rocks by being strongly depleted in HFSE, however, they also resemble MORB and volcanic arc tholeiite in the degree of LREE and LILE enrichment (Fig. 5C, D and G, H). Therefore,

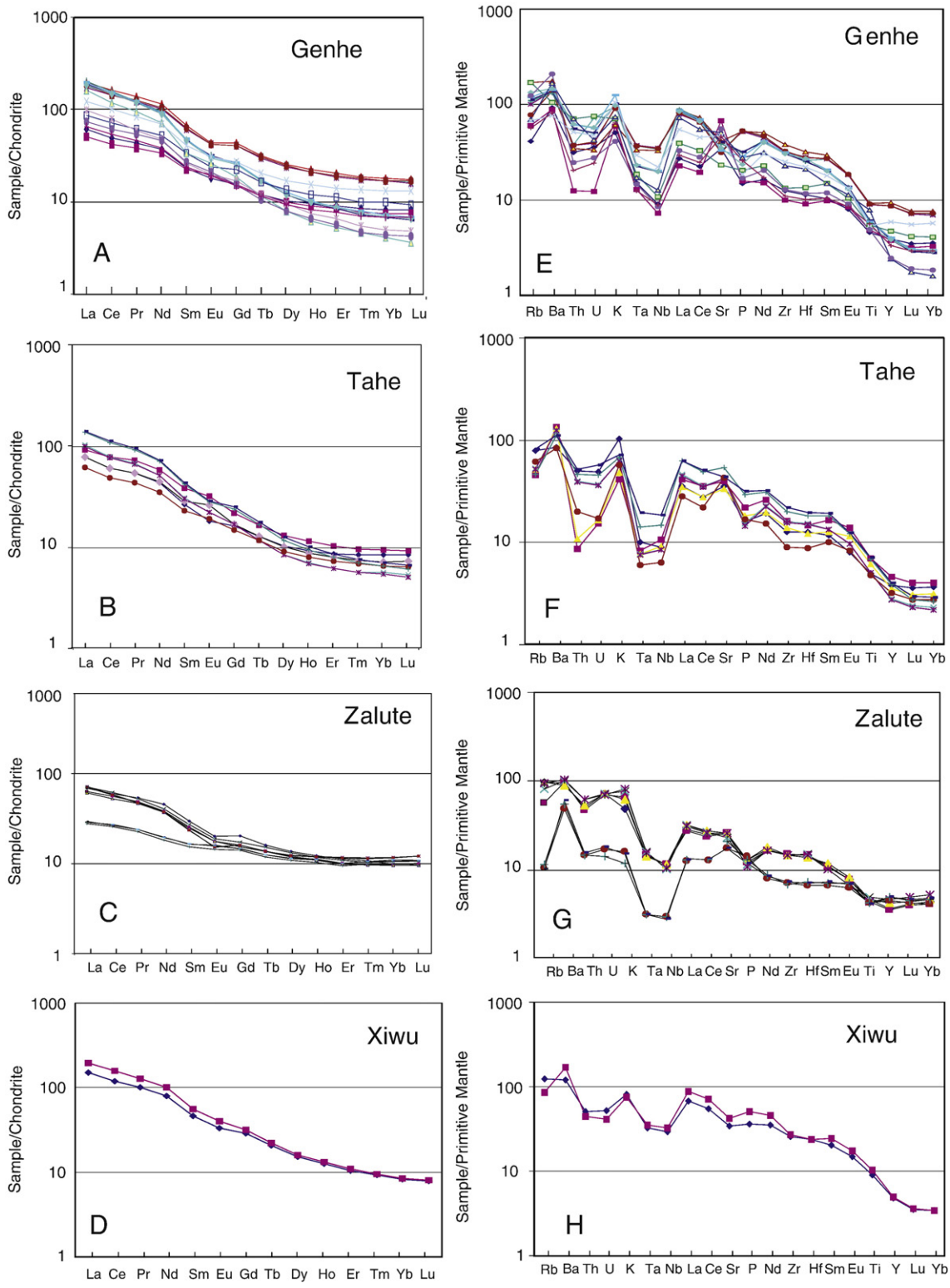

Fig. 5. (A–D) Chondrite-normalized REE element patterns for the basaltic rocks from the Great Xinggan Range. Chondrite normalizing values are from Boynton (1984). (E–H) Primordial mantle normalized multi-element patterns for the basaltic rocks from the Great Xinggan Range. Primordial mantle normalizing values are from Sun and McDonough (1989).

the Mesozoic basalts in the Great Xinggan Range have variable compositions. Recent research shows that the calc-alkaline volcanic rocks can be formed either in compressional island arcs or extensional intraplate settings. Hawkesworth et al. (1995) suggested that the generation of Cenozoic (>20 Ma) calc-alkaline magmatism in the Basin and Range Province is due to lithospheric thinning and extension. The Great Xinggan Range rocks show similar Sr contents and Zr/Y ratios to those of Cenozoic calc-alkaline volcanic rocks of the Basin and Range Province but have much higher Sr contents and Zr/Y ratios than those of island arc volcanic rocks as illustrated in Fig. 10A and B. It is noteworthy that many similarities are displayed between the Basin and Range Province and the NE China fold belt, e.g., crustal

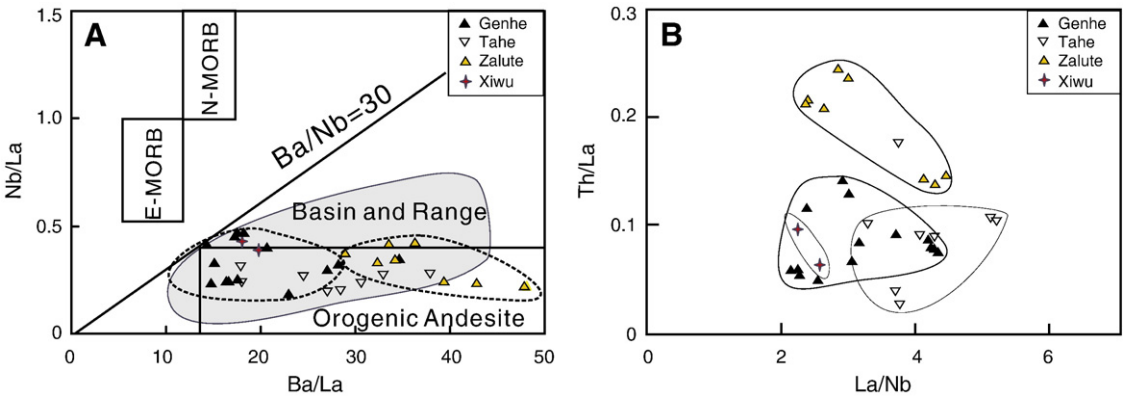

Fig. 6. (A) Ba/La vs. Nb/La and (B) Th/La vs. La/Nb variation diagrams of the Late Mesozoic basaltic rocks. All samples have lower Nb/La ratios but higher Ba/La ratios than MORB. Data source: E-MORB and N-MORB (Sun and McDonough, 1989); Basin and Range Province (Hawkesworth et al., 1995); orogenic andesites (Gill, 1981). Symbols as in Fig. 3.

extension and formation of rift-faulting basins as well as widely distributed calc-alkaline volcanism.

The anti-correlation between SiO_2 and MgO, CaO, Fe_2O_3 are compatible with fractional crystallization processes within a closed system (Fig. 4). A diagram of La content vs. La/Sm ratio of the basaltic rocks in the Great Xinggan Range also shows that the magmatic evolution is dominated by the fractional crystallization (Fig. 11).

5.2. Source characteristics

Based on the differences between the Tahe and Xiwu groups and Genhe and Zalute groups for Sr–Nd–Pb–Hf isotopic compositions elucidated above, we will evaluate their source characteristics.

5.2.1. Sources of the Tahe and Xiwu groups

It is necessary to evaluate crustal contamination or assimilation and fractional crystallization (AFC) processes for the continental volcanic rocks as they have to pass through the thick continental crust before reaching the surface. In the SiO_2 vs. initial Sr isotopic ratios and $\varepsilon_{Nd}(t)$ diagram (Fig. 12), the Tahe and Xiwu basaltic rocks show no correlation, which implies that crustal materials were not assimilated and fractional crystallization may play an important role during magma evolution. Thus, the Sr–Nd–Pb–Hf isotopic compositions may closely reflect their source features.

As mentioned above, the enrichment of LILEs and LREE and depletion of HFSE in the Tahe and Xiwu groups are similar to that of IAB, which means that the lithospheric mantle sources of the Tahe and Xiwu might have been modified by the subducted slab and these geochemical characteristics are likely to be the imprint of subduction. The Ba/Nb ratio of active continental margin magmatism is usually greater than 28 (Gill, 1981; Fitton et al., 1988). The higher Ba/Nb ratios of these volcanic rocks range between 33 and 252, which is well in excess of 28 (Fig. 6A), making these volcanic rocks quite similar to subduction related magmatism. In the Rb/Y vs. Nb/Y diagram (Fig. 13A), the volcanic rocks vary along the Rb/Y axis and confirm a subduction zone enrichment trend. In the Pb/Ce vs. Pb diagram (Fig. 13B), the basaltic rocks plot near the abyssal sediment field and also confirm a subduction zone enrichment trend.

In the $(^{87}Sr/^{86}Sr)_i$ vs. $\varepsilon_{Nd}(t)$ variation diagram (Fig. 7A), the Tahe and Xiwu samples are mainly located among PM, EM I and EM II while the Tahe samples trend towards EM II, which implies that the magma sources of the Tahe group experienced metasomatism of fluids/melts derived from the subducted slab and display an obvious imprint of the subduction of oceanic slabs. As stated above, the multiple oceanic subduction events happened during the Paleozoic to Early-Mesozoic in the eastern part of the Paleo-Asian oceans (Badarch et al., 2002; Xiao et al., 2003; Li, 2007), thus we suggest that the metasomatic

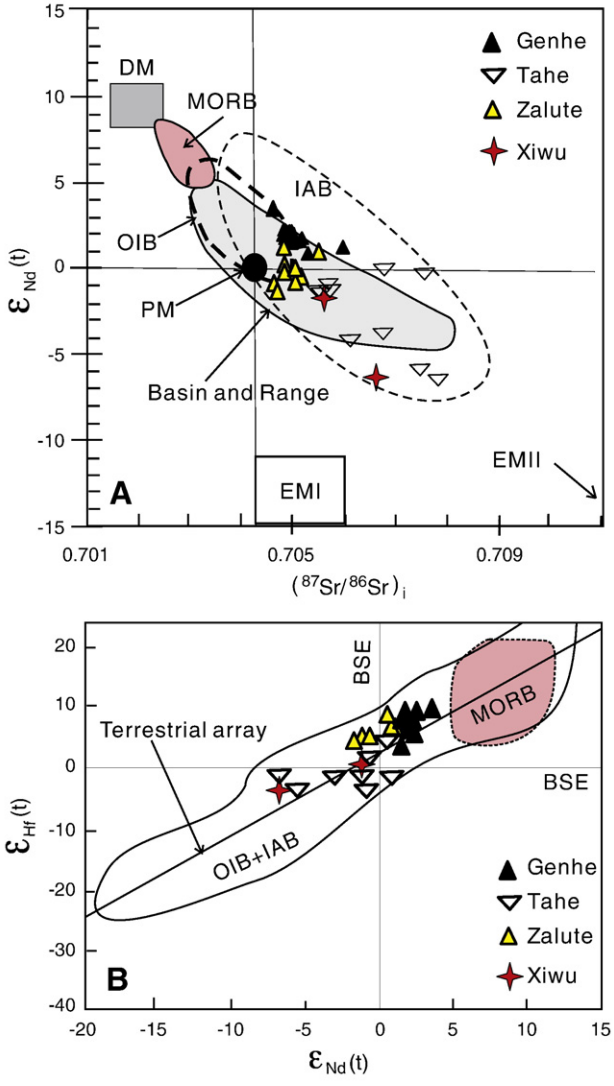

Fig. 7. (A) $(^{87}Sr/^{86}Sr)_i$ vs. $\varepsilon_{Nd}(t)$ plots of the Late Mesozoic basaltic rocks in the Great Xinggan Range. All of the rocks exhibit slightly depleted to weakly enriched Nd isotopic ratios as well as slightly enriched Sr isotopic ratios, overlapping the variation range of the Cenozoic volcanic rocks in the Basin and Range Province, USA (Hawkesworth et al., 1995; Rogers et al., 1995). PM denote primitive mantle (Zhou et al., 2001), EM I and EM II denote enriched mantle I and enriched mantle II, respectively (Zindle and Hart, 1986). (B) $\varepsilon_{Nd}(t)$ vs. $\varepsilon_{Hf}(t)$ diagram of the Late Mesozoic volcanic rocks in the Great Xinggan Range. BSE denote bulk silicate earth. Fields of the MORB, OIB, IAB and the terrestrial array from Vervoort et al. (1999).

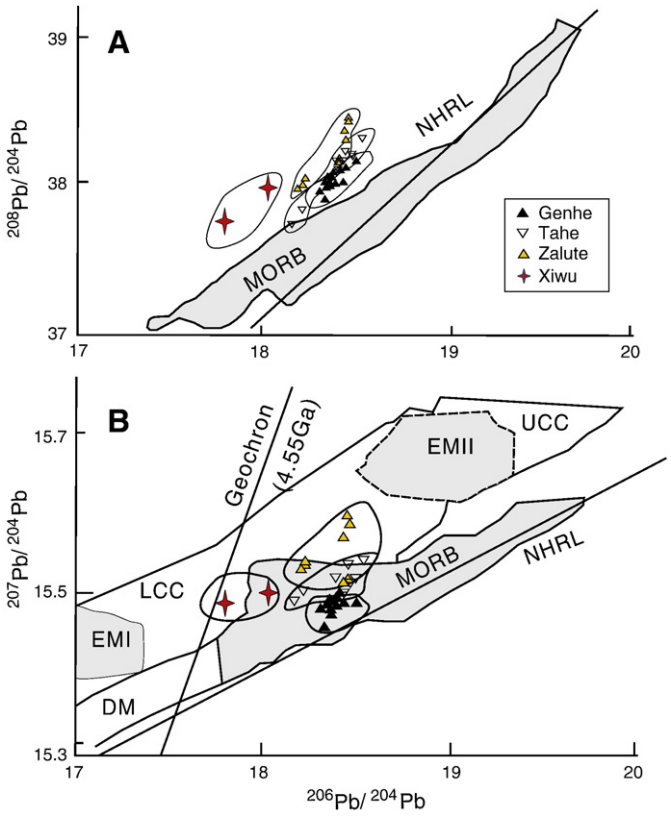

Fig. 8. (A) $^{208}Pb/^{204}Pb$ vs. $^{206}Pb/^{204}Pb$ isotope correlation diagram showing the position of the northern hemisphere reference line (NHRL) with Th/U=4.0. The field of MORB is shown with a cross-hatched pattern. (B) $^{208}Pb/^{204}Pb$ vs. $^{206}Pb/^{204}Pb$ isotope correlation diagram showing the position of the northern hemisphere reference line (NHRL), the slope of which has an age significance of 1.77 Ga. The mantle reservoirs of Zindle and Hart (1986) are plotted as follows: DM, depleted mantle; HIMU, mantle with high U/Pb radio; UCC/LCC, upper and lower continental crust (Zindle and Hart, 1986). Fields of MORB, EMI and EMII with shadow-hatching. In above figures all Pb isotopes plotting are the measured value.

components mainly derive from the fluids released from the subducting slab during the closure of the Paleo-Asian and Mongol–Okhotsk oceans.

Most intriguing about the isotopic characteristics of the basalts is the regional difference in $^{206}Pb/^{204}Pb$ ratios (Fig. 8), requiring two large-scale isotopic domains in the mantle source: PM–EM II for the Tahe, and PM–EM I for the Xiwu group. The source of EM I component seen in the Xiwu group may reflect the influence of an older block (Xilinhot-Xiwu).

5.2.2. Source of the Genhe and Zalute groups

Basaltic rocks of the Genhe and Zalute groups have lower $(^{87}Sr/^{86}Sr)_i$ (0.7046–0.7059), higher $\varepsilon_{Nd}(t)$ (−1 to +3.6), higher $\varepsilon_{Hf}(t)$ (4.1 to 8.9) and no obvious Eu anomalies (δEu=0.87–1.11) compared to the Tahe and Xiwu groups. In the SiO_2 vs. initial Sr isotopic ratio and $\varepsilon_{Nd}(t)$ diagram (Fig. 12), the Genhe and Zalute basaltic rocks exhibit no correlations and weakly negative correlation between $(^{87}Sr/^{86}Sr)_i$ vs. SiO_2 and between $\varepsilon_{Nd}(t)$ vs. SiO_2. This suggests that the magma ascended at a higher speed and was not significantly affected by crustal contamination. Thus, the Sr–Nd–Pb–Hf isotopic compositions closely reflect source compositions and mantle processes.

The Genhe and Zalute rocks plot along the correlation line between DM and EM II (Fig. 7A). This indicates that the sources of the Genhe and Zalute groups were characterized by mixing among PM, DM and EM II, and had experienced metasomatism by fluid/melt derived from the subducting plate (Fig. 13).

Some basalts in the Genhe group belong to the shoshonitic series characterized by high K_2O, and strongly enriched in LILEs and LREE. The lower Sr/Nd ratios (13.0–17.5) of basalts are similar to those of OIB, but the characteristics of Ta/Hf, Th/Ta and association with the A-type granites suggest that the shoshonites were generated in an intraplate setting, most likely a continental rift. The shoshonitic magma is considered to be the partial melting product of phlogopite-bearing lherzolite in the enriched Mesozoic lithospheric mantle (Wu et al., 2002).

5.2.3. Comparison with the Basin and Range Province

Based on the elemental and isotopic features, the volcanic rocks of the Great Xinggan Range show similarities to those from the Basin and Range Province of the western United States (Ormerod et al., 1988; Hawkesworth et al., 1995).

The geochemical investigations on the Tertiary volcanic rocks in the Basin and Range Province have implied that these rocks were generated from the lithospheric mantle in an extensional setting, and the lithospheric mantle had been metasomatized by fluids released from an ancient subduction event, rather than contemporaneous subduction like a modern arc (Pearce and Peate 1995). The volcanic rocks generated by this mechanism usually have higher Sr, Zr/Y and Na_2O contents than typical modern arc volcanic rocks. These features are also apparent in the Great Xinggan Range volcanic rocks (Fig. 10A and B).

Thus we propose that the source for the Great Xinggan Range volcanic rocks is an enriched lithospheric mantle rather than a metasomatized mantle wedge, and the enriched characteristics resulted from metasomatism by fluids derived from Paleo-subducted slabs during the closure of the Paleo-Asian and/or Mongol–Okhotsk oceans (Li, 2007).

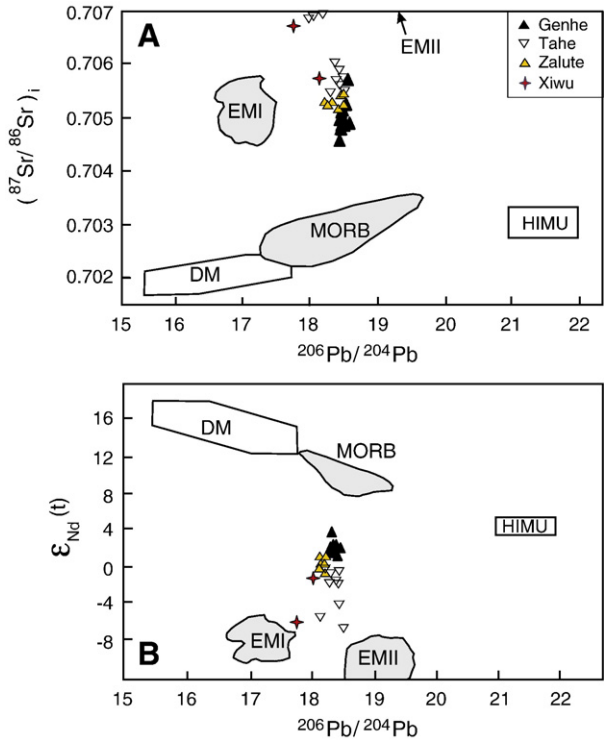

Fig. 9. (A) $^{87}Sr/^{86}Sr$ vs. $^{206}Pb/^{204}Pb$ isotope correlation diagram; (B) $\varepsilon_{Nd}(t)$ vs. $^{206}Pb/^{204}Pb$ isotope correlation diagram. Both diagrams show the positions of the mantle reservoirs identified by Zindle and Hart (1986): DM, depleted mantle; HIMU, mantle with high U/Pb ratio; UCC/LCC, upper and lower continental crust (Zindle and Hart, 1986). Fields of MORB, EMI and EMII with shadow-hatching. In above figures all Pb isotopes plotting are the measured value.

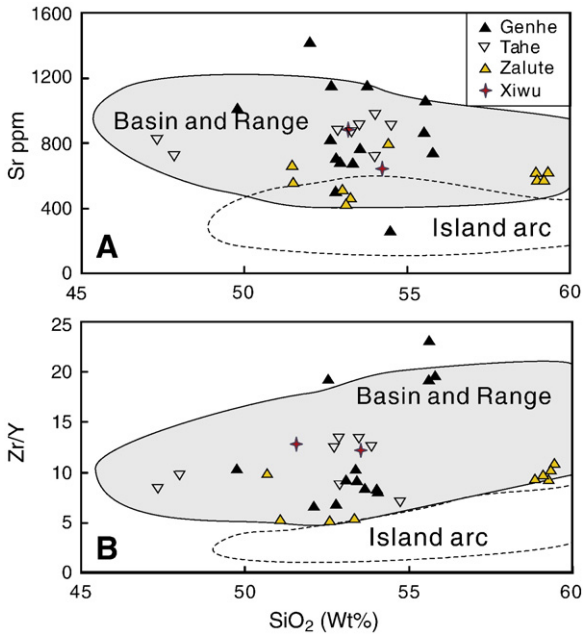

Fig. 10. (A) A comparison of Sr contents and (B) Zr/Y ratio of the Late Mesozoic volcanic rocks in the Great Xinggan Range with those of Cenozoic volcanic rocks in the Basin and Range Province and island arc volcanic rocks in Japan (Hawkesworth et al., 1995). The rocks possess similar Sr contents and Zr/Y ratios to those from Basin and Range Province the but higher than those from island arc volcanic rocks.

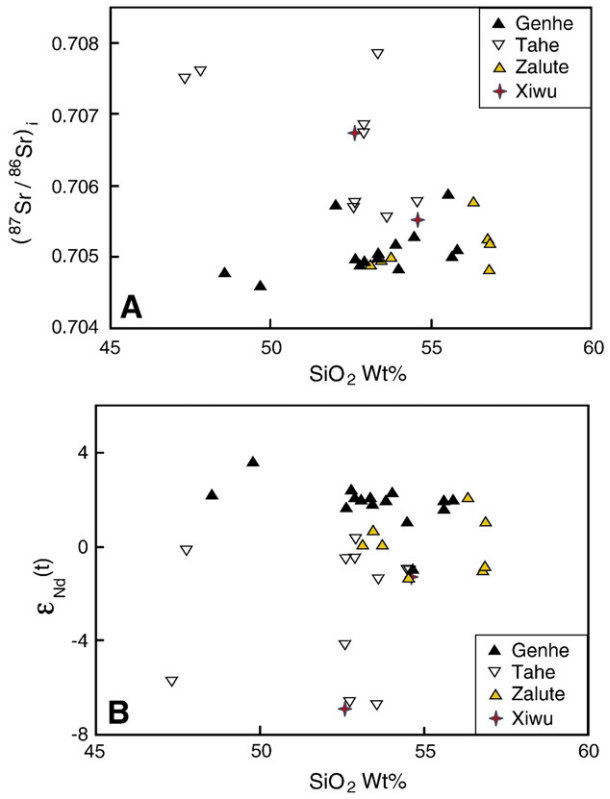

Fig. 12. (A) SiO_2 vs. $(^{87}Sr/^{86}Sr)_i$ and (B) SiO_2 vs. $\varepsilon_{Nd}(t)$ diagrams. All basaltic rocks exhibit not correlation and weakly negative correlation between $(^{87}Sr/^{86}Sr)_i$ and SiO_2 and between $\varepsilon_{Nd}(t)$ and SiO_2. These indicate no involvement of crustal materials and an important role of fractional crystallization during magma evolution.

5.3. Tectonic setting

The tectonic setting of the Great Xinggan Range in the Early Cretaceous has been hotly debated since the 1980s. A mantle plume hypothesis (Lin et al., 1998; Ge et al., 1999), post-orogenic diffuse extension (Fan et al., 2003), and an active continental margin related to subduction of the Paleo-Pacific Plate beneath the Asia continent (Zhao et al., 1989, Faure and Natal'in, 1992; Zhao et al., 1994) have been proposed.

Lin et al. (1998) and Ge et al. (1999) noted that the extensive Late Mesozoic magmatism in the Great Xinggan Range was induced by an upwelling mantle plume on the basis of the large-scale and ring-like distributive basaltic lavas in the region. However, existence of an upwelling mantle plume is unlikely for the following reasons: Firstly, OIB-like basaltic rocks are lacking in the Great Xinggan Range; secondly, recently published geochronological data indicate that ages of the volcanic eruption in this region is characterized by migration from west to east (160 Ma to 125 Ma, Wang et al., 2006), which is inconsistent with the rapid manner of magma generation and eruption caused by an upwelling mantle plume.

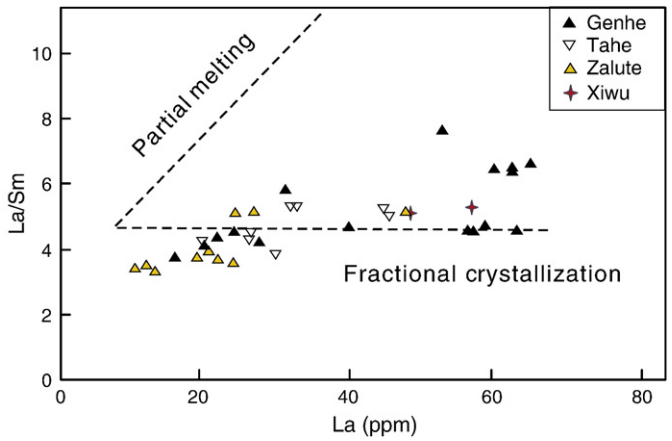

Fig. 11. La vs. La/Sm diagram of the Late Mesozoic volcanic rocks in the Great Xinggan Range. It is shown that the magmatic evolution is dominated by the fractional crystallization.

Fan et al. (2003) and Meng (2003) suggested that the Mesozoic volcanic rocks in the Great Xinggan Range were formed due to subduction of the Mongol–Okhotsk ocean and subsequent orogenic extension and collapse. Although it might be argued that the Jurassic basalt, exposed in the western part of the Great Xinggan Range, might be related to the subduction and closure of the Mongol–Okhotsk ocean, the Early Cretacous basalts of the main Great Xinggan Range do not support this interpretation. If the Early Cretacous rocks in the Great Xinggan Range are considered as the product of post-orogenic evolution, it is difficult to explain why these rocks extend in a NNE direction, not in a E–W direction parallel to the Mongol–Okhotsk suture (Fig. 2). Moreover, as we will discuss below, Mesozoic volcanic rocks are widely distributed in the main continental area of eastern China, which cannot be explained by the collapse of the Mongol–Okhotsk Orogen.

Another hypothesis of invoking an active continental margin proposed that some characteristics of the Great Xinggan Range volcanic rocks are similar to those of continental marginal island arcs (Engebretson et al., 1985; Faure and Natal'in, 1992; Zhao et al., 1994; Zhang et al., 2008). The chemical compositions of the Great Xinggan Range rocks do not show typical features of the arc volcanic rocks, the incompatible element abundances are also higher than those of the arc magmas, therefore, it is difficult to explain the tectonic environment through a direct relation to Pacific plate subduction.

As we discussed above, the geochemical characteristics of the Late Mesozoic volcanic rocks in the Great Xinggan Range resemble those of the Cenozoic calc-alkaline magmatism in the Basin and Range Province of the United States. Combined with the formation period of the A-granite (Wu et al., 2002), the calc-alkaline volcanic rocks have

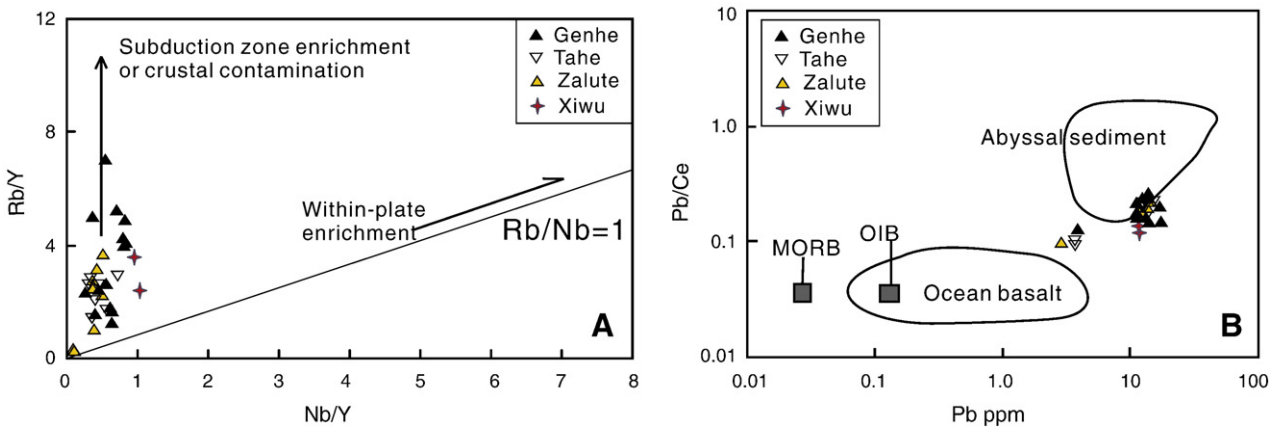

Fig. 13. (A) Rb/Y vs. Nb/Y diagram (Temel et al., 1998), the volcanic rocks vary along the Rb/Y axis and confirm a subduction zone enrichment trend. (B) Pb/Ce vs. Pb diagram (Othman et al., 1989), all basaltic rocks plot near the abyssal sediment field.

been interpreted as the products of the decompressional partial melting of metasomatized lithospheric mantle due to the lithospheric extension and thinning. Here we prefer that the widespread Mesozoic volcanic rocks in the Great Xinggan Range region were generated in an extensional regime, but this extensional regime is mainly attributed to asthenospheric upwelling and distant effect of subduction of the Paleo-Pacific plate in the east China.

This paper supports the hypothesis of a shears-shaped delamination mechanism for the geodynamic setting beneath northeast Asia in the Late Mesozoic suggested by Wang et al. (2006). The Asian continent obstructed the westwards movement of the region from the subduction of the Paleo-Pacific plate, causing a rise of strain in the lithosphere and finally resulting in a shears-like lithospheric delamination starting from the west of the Great Xinggan Range around 160 Ma and then extended gradually eastwards. This led to mantle upwelling and underplating, resulting small-scale magmatic activity in the western Great Xinggan Range in the Late Jurassic and large-scale volcanism in main the Great Xinggan Range in the Early Cretaceous.

6. Conclusions

The Mesozoic basaltic rocks in the Great Xinggan Range are dominated by an Early Cretaceous calc-alkaline series with subordinate alkaline series rocks in the northern Great Xinggan Range. These rocks include trachytic basalts, basalts, and basaltic andesites.

The volcanic rocks are characterized by significant LILEs and LREE enrichment and HFSE depletion. The Genhe and Tahe basalts exhibit a strong depletion in Nb and Ta, and a selective enrichment in HFSE, similar to the alkaline basalts formed in a volcanic arc. The Zalute and Xiwu basalts show a slight depletion in Nb and Ta and high Th/Ta ratio, resembling basalts formed in an intraplate extensional zone.

The mantle sources for the Great Xinggan Range basaltic rocks are heterogeneous. The Tahe and Xiwu regions are characterized by weakly enriched lithospheric mantle. The Genhe and Zalut basaltic rocks exhibit very similar and slightly enriched Sr and weakly depleted to slightly enriched Nd isotopic ratios, which seems to suggest that the sources for the those rocks are a weakly depleted to enriched continental lithospheric mantle. We suggest that the mantle sources of the Genhe and Zalute groups are characterized by mixing among PM, EM II and DM, whereas the Tahe and Xiwu groups are characterized by enriched lithospheric mantle which experienced metasomatism by fluid/melt derived from the subducted Paleo-Asian and/or Mongol–Okhotsk Ocean slab and a contribution from older lithosphere.

The Early Cretaceous volcanic rocks in the Great Xinggan Range were generated in an extensional tectonic setting, which is similar to that for the Cenozoic volcanic rocks in Basin and Range Province of the United States.

Acknowledgements

This paper is supported by the National Natural Science Foundation of China (Grants No. 40334043) and Major State Basic Research Program of the People's Republic of China (No.2006CB403507). J.A., Shao and W.M. Fan are thanked for beneficial discussions. We appreciate F.K. Chen, X.D. Jin and H. Li for their help with chemical and isotope analysis. Q. Liu and Y.T. Zhang are thanked for their assistance in the fieldwork. We are grateful to two anonymous reviewers for the constructive reviews, which greatly improved the original manuscript. The authors appreciate the efforts of Walter I. for his improvement of the English.

Appendix A. Supplementary data

Supplementary data associated with this article can be found, in the online version, at doi:10.1016/j.chemgeo.2008.07.004.

References

Badarch, G., Dickson, C.W., Windley, B.F., 2002. A new terrane subdivision for Mongolia: implications for the Phanerozoic crustal growth of Central Asia. J. Asian Earth Sci. 21, 87–110.
Bizzarro, M., Baker, J., Ulfbeck, D., 2003. A new digestion and chemical separation technique for rapid and highly reproducible determination of Lu/Hf and Hf isotope ratios in geological materials by MC-ICPMS. Geostand. Newsl. 27, 133–145.
Boynton, W.V., 1984. Geochemistry of the rare earth elements: meteorite studies. In: Henderson, P. (Ed.), Rare Earth Element Geochemistry. Elsevier, pp. 63–114.
Chen, Y., Chen, W., Zhou, X.H., 1997. Mesozoic Volcanic Rocks: Chronology, Geochemistry and Tectonic Background. Seimology Press, Beijing. 279pp.
Chen, B., Jahn, B.M., Wilde, S., Xu, B., 2000. Two contrasting Paleozoic magmatic belts in northern Inner Mongolia, China: petrogenesis and tectonic implications. Tectonophy 328, 157–182.
Chen, Z.G., Zhang, L.C., Zhou, X.H., Wan, B., Ying, J.F., Wang, F., 2006. Geochronology and geochemical characteristics of Mesozoic volcanic rocks section in Manzhouli Xinyouqi, Inner-Mongolia. Acta Petrol. Sin. 22, 2971–2987 (in Chinese with English abstract).
Davis, G.A., Zheng, Y., Wang, C., Darby, B.J., Zhang, C., Gehrels, G., 2001. Mesozoic tectonic evolution of the Yanshan fold and thrust belt, with emphasis on Hebei and Liaoning provinces, Northern China. In: Hendrix, M.S., Davis, G.A. (Eds.), Paleozoic and Mesozoic Tectonic Evolution of Central Asia: From Continental Assembly to Intracontinental Deformation. Geol. Soc. Am. Mem., vol. 194, pp. 171–198.
Deng, J., Mo, X., Zhao, H., 2004. A new model for the dynamic evolution of Chinese lithosphere: continental root plume tectonics. Earth Sci. Rev. 65, 223–275.
Engebretson, D.C., Cox, A., Gordon, R.G., 1985. Relative motions between oceanic and continental plates in the Pacific basin. Geol. Soc. Am. Spec. Paper 206, 1–59.
Fan, W.M., Guo, F., Wang, Y., Ge, L., 2003. Late Mesozoic calc-alkaline volcanism of post-orogenic extension in the northern Dahinggan Mountains, northeastern China. J. Volcanol. Geotherm. Res. 121, 115–135.
Faure, M., Natal, ' in, B., 1992. The geodynamic evolution of the eastern Eurasian margin in Mesozoic times. Tectonophys 208, 397–411.
Fitton, J.G., James, D., Kempton, P.D., Ormerod, D.S., Leeman, W.P., 1988. The role of lithospheric mantle in the generation of Late Cenozoic basic magmas in the western United States. J. Petrol. 331–349 special volume (special lithosphere issue).
Ge, W., Lin, Q., Sun, D., 1999. Geochemical characteristics of the Mesozoic basalts in DaXinggan evidence of the mantle–crust interaction. Acta Petrol. Sin. 15, 396–407 (in Chinese with English abstract).

Gill, J.B., 1981. Orogenic Andesites and Plate Tectonics. Springer-Verlag, New York, p. 310.
Hawkesworth, C.J., Turner, S., Gallagher, K., Hunter, A., Bradshaw, T., Rogers, N., 1995. Calc-alkaline magmatism, lithosphere thinning and extension in the Basin and Range. J. Geophys. Res. 100, 10271–10286.
Irvine, T.N., Baragar, W.R.A., 1971. A guide to the chemical classification of the common volcanic rocks. Can. J. Earth. Sci. 8, 523–528.
Jahn, B.M., Wu, F., Capdevila, R., Fourcade, S., Wang, Y., Zhao, Z., 2001. Highly evolved juvenile granites with tetrad REE patterns: the Woduhe and Baerzhe granites from the Great Xing'an (Khingan) Mountains in NE China. Lithos 59, 171–198.
Jahn, B.M., Windley, B., Natal, ' in, B., Dobretsov, N., 2004. Phanerozoic continental growth in Central Asia. J. Asian Earth Sci. 23, 599–603.
Kleinhanns, I.C., Kreissig, K., Kamber, B.S., 2002. Combined chemical separation of Lu, Hf, Sm, Nd, and REEs from a single rock digest: precise and accurate isotope determinations of Lu–Hf and Sm–Nd using multicollector-ICPMS. Anal. Chem. 74, 67–73.
Kovalenko, V.I., 2004. Isotope provinces, mechanisms of generation and source of the continental crust in the Central Asia mobile belt: geological and isotopic evidence. J. Asian Earth Sci. 23, 605–627.
Kravchinsky, V.A., Cogne, J.P., Harbert, W.P., Kuzmin, M.I., 2002. Evolution of the Mongol–Okhotsk Ocean as constrained by new palaeomagnetic data from the Mongol–Okhotsk suture zone, Siberia. Geophys. J. Int. 148, 34–57.
Le Bas, M., Le Maitre, R.W., Streckeisen, A., Zanettin, B., 1986. A chemical classification of volcanic rocks based on the total-silica diagram. J. Petrol. 27, 745–750.
Li, J.Y., 2007. Permian geodynamic setting of Northeast China and adjacent regions: closure of the Paleo-Asian Ocean and subduction of the Paleo-Pacific Plate. J. Asian Earth Sci. 26, 207–224.
Li, X.H., Qi, C.S., Liu, Y., 2005. Rapid separation of Hf from rock samples for isotope analysis by MC-ICPMS: a modified single-column extraction chromatography method. Geochimica 34, 109–114.
Lin, Q., Ge, W., Sun, D., 1998. Tectonic significance of Mesozoic volcanic rocks in northeastern China. Sci. Geol. Sin. 33, 129–139 (in Chinese with English abstract).
Meng, Q., 2003. What drove late Mesozoic extension of the northern China–Mongolia tract? Tectonophysics 369, 155–174.
Mueller, J.F., et al., 1991. Late Carboniferous to Permian sedimentation in Inner Mongolia, China, and tectonic relationships between North China and Siberia. J. Geol. 99, 251–263.
Ormerod, D.S., Hawkesworth, C.J., Rogers, N.W., Leeman, W.P., Menzies, M.A., 1988. Tectonic and magmatic transitions in the Western Great Basin, U.S.A. Nature 333, 349–353.
Othman, D.B., White, W.M., Patchett, J., 1989. Geochemistry of marine sediments, island arc magma genesis and crust–mantle recycling. Earth Planet. Sci. Lett. 94, 12–21.
Pearce, J.A., Peate, D.W., 1995. Tectonic implications of the composition of volcanic arc magmas. Ann. Rev. Earth Planet. Sci. 23, 251–285.
Rogers, N.W., Hawkesworth, C.J., Ormerod, D.S., 1995. Late Cenozoic basaltic magmatism in the western Great-Basin, California and Nevada. J. Geophys. Res.-Solid Earth 100, 10287–10301.
Shao, J.A., Zang, S.X., Mou, B.L., 1994. Extensional tectonics and asthenospheric upwelling in the orogenic belt: a case study from Hinggan-Mongolia Orogenic belt. Chin. Sci. Bull. 39, 533–537.
Shao, J., Mu, B., Zhang, L., 2000. Deep geological process and its shallow response during Mesozoic transfer of tectonic framework in eastern North China. Geol. Rev. 46, 32–40 (in Chinese with English abstract).
Smedley, P.L., 1986. The relationship between calc-alkaline volcanism and within-plate continental rift volcanism: evidence from Scottish Palaeozoic lavas. Earth Planet. Sci. Lett. 76, 113–128.
Song, J., Dou, L., 1997. Mesozoic–Cenozoic Tectonics of Petroliferous Basins in Eastern China and their Petroleum Systems. Petroleum Industry Press, Beijing. 182 pp.
Sun, S., McDonough, W.F., 1989. Chemical and isotopic systematics of oceanic basalts: implications for mantle composition and processes. In: Saunders, A.D., Norry, M.J. (Eds.), Magmatism in the Ocean Basins. Geological Society (London), vol. 42, pp. 313–345. Special Publication.
Temel, A., Gtlndogdu, M.N., Gourgaud, A., 1998. Petrological and geochemical characteristics of Cenozoic high-K calc-alkaline volcanism in Konya, Central Anatolia, Turkey. J. Volcanol. Geotherm. Res. 85, 327–354.
Tomurtogoo, O., Windley, B.F., Kroner, A., Badarch, G., Liu, D.Y., 2005. Zircon age and occurrence of the Adaatsag ophiolite and Muron shear zone, central Mongolia: constraints on the evolution of the Mongol–Okhotsk ocean, suture and orogen. J. Geol. Soc. 162, 125–134.
Van der Voo, R., Spakman, W., BijWaard, H., 1999. Mesozoic subducted slabs under Siberia. Nature 397, 246–249.
Vervoort, J., Patchett, P.J., Blichert-Toft, J., 1999. Relationships between Lu–Hf and Sm–Nd isotopic systems in the global sedimentary system. Earth Planet. Sci. Lett. 168, 79–99.
Wang, F., Zhou, X.H., Zhang, L.C., Ying, J.F., Wu, F.Y., Zhu, R.X., 2006. Late Mesozoic volcanism in the Great Xing'an Range (NE China): timing and implications for the dynamic setting of NE Asia. Earth Planet. Sci. Lett. 251, 179–198.
Wu, F., Sun, D., Lin, D., 1999. Petrogenesis of the Phanerozoic granites and crustal growth in the northeast China. Acta Petrol. Sin. 15, 181–189.
Wu, F., Sun, D.Y., Li, H.M., Jahn, B.M., Wilde, S.A., 2002. A-type granites in Northeastern China: age and geochemical constraints on their petrogenesis. Chem. Geol. 187, 143–173.
Wu, F., Lin, J., Wilde, S.A., Zhang, X., Yang, J., 2005. Nature and significance of the Early Cretaceous giant igneous event in eastern China. Earth Planet. Sci. Lett. 233, 103–119.
Xiao, W.J., Windley, B.F., Hao, J., Zhai, M.G., 2003. Accretion leading to collision and the Permian Solonker suture, Inner Mongolia, China: termination of the central Asian orogenic belt. Tectonics 22, 1069. doi:10.1029/2002TC001484.
Xie, X., Yan, M., Li, L., Shen, H., 1989. Usable values for Chinese standard reference samples of stream sediments, soils, and rocks: GSD 9-12, GSS 1-8 and GSR 1-6. Geostandards. Newsletter 9, 277–280.
Yarmolyuk, V.V., Kovalenko, V.I., 2001. The Mesozoic–Cenozoic of Mongolia. In: Dergunov, A.B. (Ed.), Tectonics, Magmatism, and Metallogeny of Mongolia. Taylor and Francis Group, London, pp. 203–244.
Zhang, J.H., Ge, W.C., Wu, F.Y., Simon, A.W., Yang, J.H., Liu, X.M., 2008. Large-scale Early Cretaceous volcanic events in the northern Great Xing'an Range, Northeastern China. Lithos 102, 138–157.
Zhao, G.L., Yang, G.L., Fu, J.Y., 1989. Mesozoic Volcanic Rocks in the Central-southern Da Hinggan Mts. Beijing Press of Science and Technology, Beijing. 155 pp. (in Chinese).
Zhao, Y., Yang, Z., Ma, X., 1994. The important age of tectonic transformation from Paleo-Asian to the Pacific tectonic domains in the East Asia. Sci. Geol. Sin. 29, 105–119 (in Chinese with English abstract).
Zhou, X.H., Zhang, G.H., Yang, J.H., Chen, W.J., Sun, M., 2001. Sr–Nd–Pb isotope mapping of Late Mesozoic volcanic rocks across northern margin of North China Craton and implications to geodynamic processes. Geochomica 30, 10–23 (in Chinese with English abstract).
Zindle, A., Hart, S.R., 1986. Chemical geodynamics. Ann. Rev. Earth Planet. Sci. 14, 493–571.
Zorin, Y.A., 1999. Geodynamics of the western part of the Mongolia–Okhotsk collisional belt, Trans-Baikal region (Russia) and Mongolia. Tectonophy 306, 33–56.